Metal coordination governs the antimicrobial efficacy of calcitermin derivatives

Silvia Leveraro,[a] Kinga Garstka,[b] Paulina Śliwka,[c] Tomasz Janek,[c] Magdalena Rowińska-Żyrek,[b] Maurizio Remelli,[a] Denise Bellotti *[a]

[a.] *Department of Chemical, Pharmaceutical and Agricultural Sciences, University of Ferrara, Via L. Borsari 46, 44121, Ferrara, Italy.*
[b.] *Faculty of Chemistry, University of Wrocław, F. Joliot-Curie 14, 50-383, Wrocław, Poland.*
[c.] *Department of Biotechnology and Food Microbiology, Wrocław University of Environmental and Life Sciences, Chełmońskiego 37, 51-630 Wrocław, Poland.*
** Corresponding author.*

Supplementary Information

1. Formation of metal complexes with WT(8-15)

Ligand protonation

The **WT(8-15)** (Ac-AHYHTHKE-NH_2) fragment has the N- and C-terminal ends modified through acetylation and amidation, respectively. This peptide corresponds to the fragment 8-15 of wild-type calcitermin with protection at both ends. Once completely deprotonated, it bears a double negative charge (L^{2-}). Six different species have been detected in solution, arising from the protonation of the following sites: three histidines, the phenolic group of tyrosine, the glutamic acid and one lysine. The Glu residue has the lowest log*K* value (3.38), and it is followed by the deprotonation of three histidine residues with log*K* values ranging from 5.21 to 6.73. Under alkaline condition, the tyrosine residue deprotonates with a log*K* value of 9.36. Finally, the last deprotonation step corresponds to the release of a proton from the protonated lysine residue (log*K* value of 10.73). The obtained protonation constants are consistent with those determined for WT calcitermin with protection at both ends.[1]

Table S1. Overall (*β*) and step (*K*) protonation constants for the ligand **WT(8-15)** at *T*= 298 K and *I*=0.1 M (KCl). Standard deviations on the last significant figure are reported in parentheses.

Ac-AHYHTHKE-NH_2 (**WT(8-15)**)			
Species	**log*β***	**log*K***	**Group/Residue**
HL^-	10.73(3)	10.73	Lys
H_2L	20.10(4)	9.36	Tyr
H_3L^+	26.83(6)	6.73	His
H_4L^{2+}	33.19(6)	6.36	His
H_5L^{3+}	38.40(8)	5.21	His
H_6L^{4+}	41.8(1)	3.38	Glu

Cu^{2+} and Zn^{2+} complexes

The formation constants of copper complexes in solution with the peptide **WT(8-15)** are reported in Table S1. The first formed complex, detected around pH 3 (Figure S4), is $[CuH_3L]^{3+}$; the stoichiometry of this species indicates that three acid-base sites are already deprotonated. It is conceivable that the coordination mode involves the imidazole nitrogens of two histidine residues ($2N_{Im}$). The complex reaches its maximum of formation around pH 4.7 and the obtained wavelength of maximum absorption (λ_{max} = 685 nm; Figure S18) perfectly fits the expected value for a coordination ($2N_{Im}$) (expected λ_{max} = 685 nm).[2, 3] In this pH range, the carboxyl group of glutamic acid is already deprotonated without being involved in complexation. Increasing the pH value, the complex $[CuH_3L]^{3+}$ deprotonates, forming the $[CuH_2L]^{2+}$ species; the corresponding pK_a value (5.07) is attributable to the deprotonation and coordination of the third histidine residue (coordination mode $3N_{Im}$). Increasing the pH, the deprotonation and coordination of two amide nitrogens of the peptide backbone give rise to the species $[CuHL]^+$ and [CuL]; the former has a maximum of formation (about 40%)

at pH 6.3, and the latter is predominant in solution in the pH range 6.6–9.3. We therefore suggest a coordination mode ($2N_{Im}$, 2N-) for the [CuL] species. This is also confirmed by the excellent agreement between the experimental and expected wavelength of maximum absorption (539 and 540 nm, respectively,[2, 3] at pH 8) (Figure S18). Further increasing the pH value, the coordination mode does not change because tyrosine deprotonates without being involved in complexation. The obtained species $[CuH_{-1}L]^-$ releases a third amidic proton with a pK_a value of 10.45 forming a complex with coordination (N_{Im}, $3N^-$). Lastly, lysine most likely spontaneously deprotonates without being involved in complexation.

Five distinct species with 1:1 stoichiometry are instead formed with Zn^{2+}. The formation of zinc complexes in solution begins around pH 5 with the first detected complex being $[ZnH_2L]^{2+}$. The stoichiometry of the complex suggests that three histidine and the glutamic acid are already deprotonated ad most likely coordinated to the metal ion ($3N_{Im}$, COO^-). Increasing the basicity of the solution, two further deprotonation steps occur, attributable to the ionization of two water molecules (pK_a values of 7.43 and 8.24). The formation *pattern* of the zinc-complexes with **WT(8-15)** is analogous to that described in the manuscript for **A7S**, **A8S** and **A7S/A8S**, with very similar calculated pK_a values. This confirms a similar behavior in its interaction with the zinc ion. Such assumption can be done also when comparing **WT(8-15)** complex formation constants with those of protected wild-type calcitermin.[1] In the most alkaline pH range, the release of two further protons leads to the formation of the $[ZnH_{-1}L]^-$ and $[ZnH_{-2}L]^{2-}$ species. The corresponding pK_a values (9.74 and 10.76) suggest the deprotonation of tyrosine and lysine residues, respectively, without being involved in complexation.

Table S2. Equilibrium constants and proposed coordination modes for Cu^{2+} and Zn^{2+} complexes with **WT(8-15)** at T = 298 K and I = 0.1 M (KCl). Values in parentheses are standard deviations on the last significant figure.

Ac-AHYHTHKE-NH_2 (**WT(8-15)**)			
Species	**logβ**	**pK_a**	**Coordination**
$[CuH_3L]^{3+}$	32.96(3)	5.07	$2N_{Im}$
$[CuH_2L]^{2+}$	27.89(3)	6.27	$3N_{Im}$
$[CuHL]^{+}$	21.62(5)	6.55	$3N_{Im}$, N^-
[CuL]	15.07(4)	9.31	$2N_{Im}$, $2N^-$
$[CuH_{-1}L]^{-}$	5.77(6)	10.45	$2N_{Im}$, $2N^-$
$[CuH_{-2}L]^{2-}$	-4.68(6)	10.78	$1N_{Im}$, $3N^-$
$[CuH_{-3}L]^{3-}$	-15.46(7)	-	$1N_{Im}$, $3N^-$
$[ZnH_2L]^{2+}$	24.88(3)	7.43	$3N_{Im}$, COO^-
$[ZnHL]^{+}$	17.45(5)	8.24	$3N_{Im}$, OH^-
[ZnL]	9.20(5)	9.74	$2N_{Im}$, $2OH^-$
$[ZnH_{-1}L]^{-}$	-0.53(6)	10.76	$2N_{Im}$, $2OH^-$
$[ZnH_{-2}L]^{2-}$	-11.29(7)	-	$2N_{Im}$, $2OH^-$

2. Speciation diagrams of metal complexes

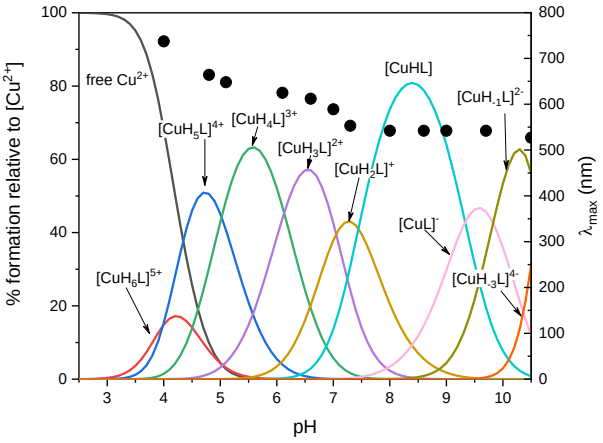

Figure S1. Representative species distribution diagram of Cu^{2+} / **A7S**; C_L=0.5 mM; M:L ratio 0.8:1. Dots correspond to the wavelength of maximum absorption of the same solution as a function of pH.

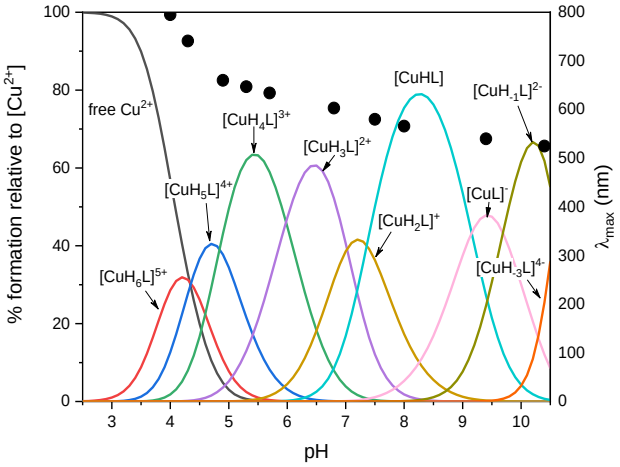

Figure S2. Representative species distribution diagram of Cu^{2+} / **A8S**; C_L=0.5 mM; M:L ratio 0.8:1. Dots correspond to the wavelength of maximum absorption of the same solution as a function of pH.

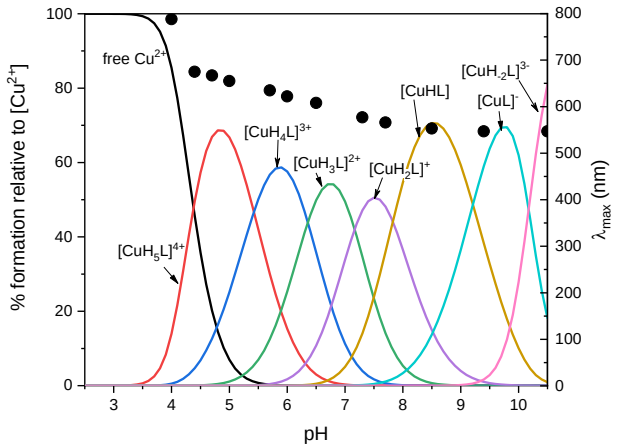

Figure S3. Representative species distribution diagram of Cu^{2+} / **A7S/A8S**; C_L=0.5 mM; M:L ratio 0.8:1. Dots correspond to the wavelength of maximum absorption of the same solution as a function of pH.

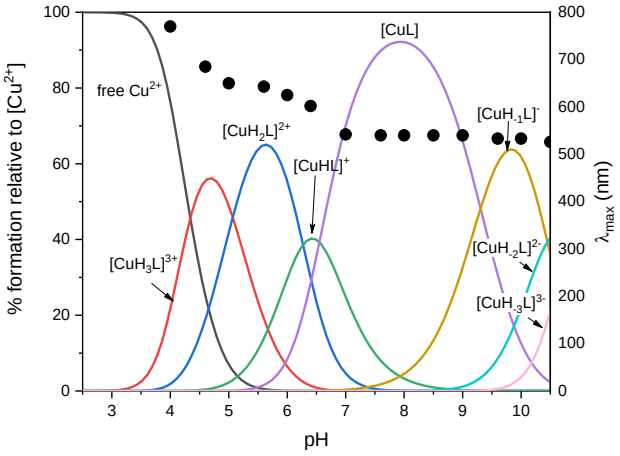

Figure S4. Representative species distribution diagram of Cu^{2+} / **WT(8-15)**; C_L=0.5 mM; M:L ratio 0.8:1. Dots correspond to the wavelength of maximum absorption of the same solution as a function of pH.

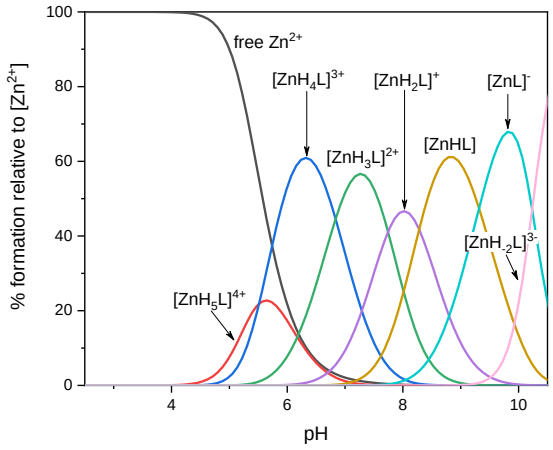

Figure S5. Representative species distribution diagram of Zn^{2+} / **A7S**; C_L=0.5 mM; M:L ratio 0.8:1.

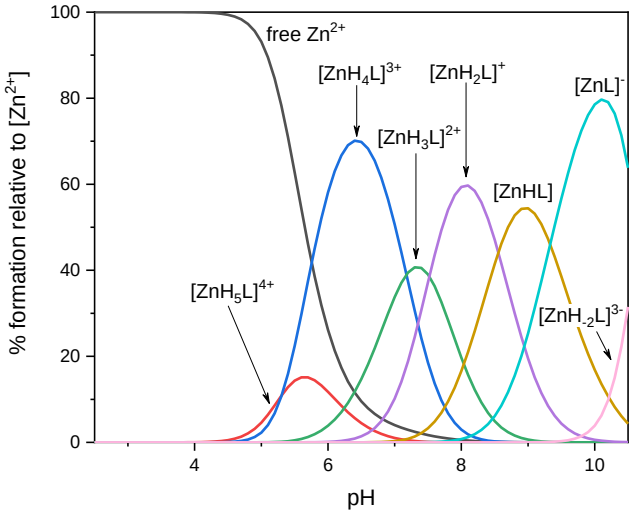

Figure S6. Representative species distribution diagram of Zn^{2+} / **A8S**; C_L=0.5 mM; M:L ratio 0.8:1.

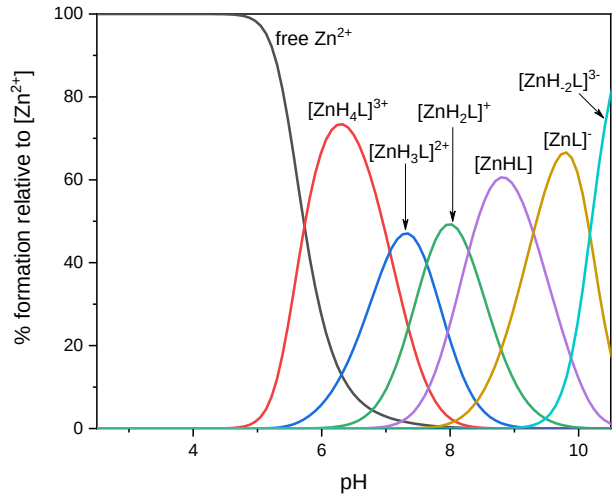

Figure S7. Representative species distribution diagram of Zn^{2+} / **A7S/A8S**; C_L=0.5 mM; M:L ratio 0.8:1.

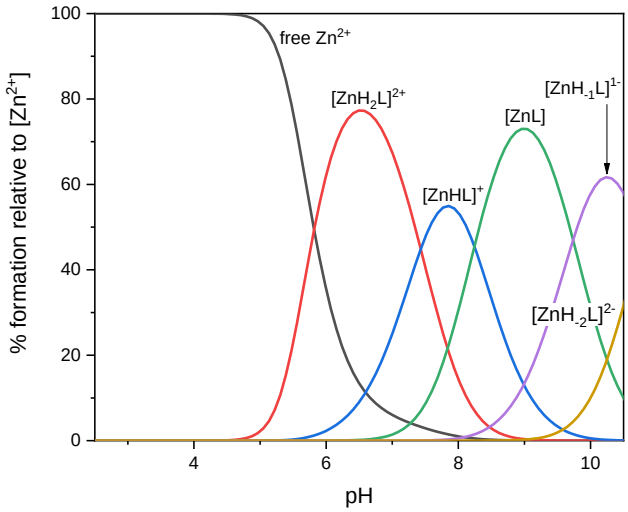

Figure S8. Representative species distribution diagram of Zn^{2+} / **WT(8-15)**; C_L=0.5 mM; M:L ratio 0.8:1.

3. Spectroscopic data: UV-Vis, CD and EPR

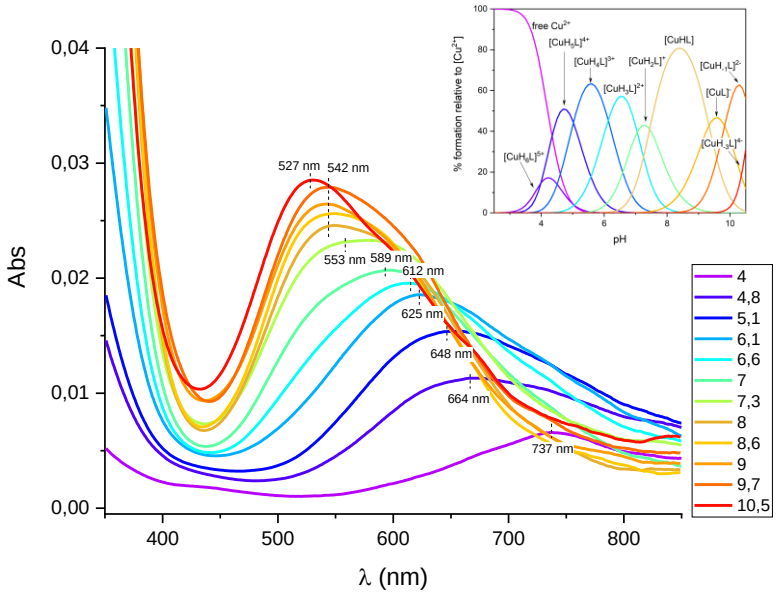

Figure S9. Vis absorption spectra of Cu^{2+} complexes with **A7S** at different pH values; M:L 0.8:1. $C_M = 0.28 \cdot 10^{-3}$ M, optical path 1 cm. The wavelength of maximum absorption is reported for each Vis absorption spectrum.

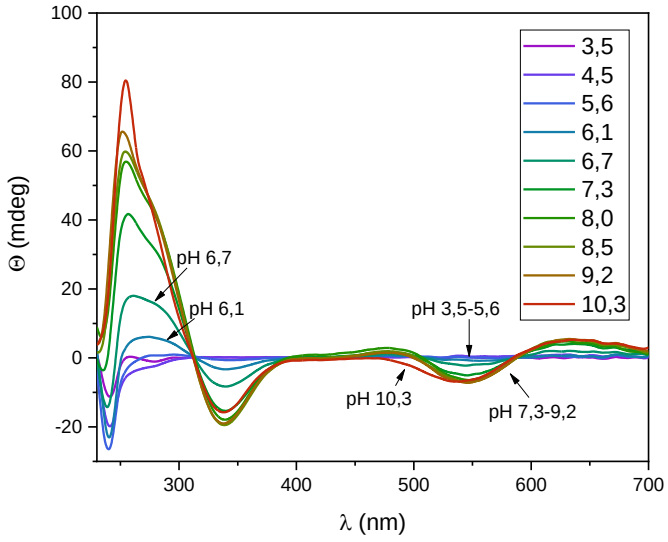

Figure S10. CD spectra of Cu^{2+} complexes with **A7S** at different pH values; M:L ratio 0.8:1, $C_M = 0.40 \cdot 10^{-3}$ M, optical path 1 cm.

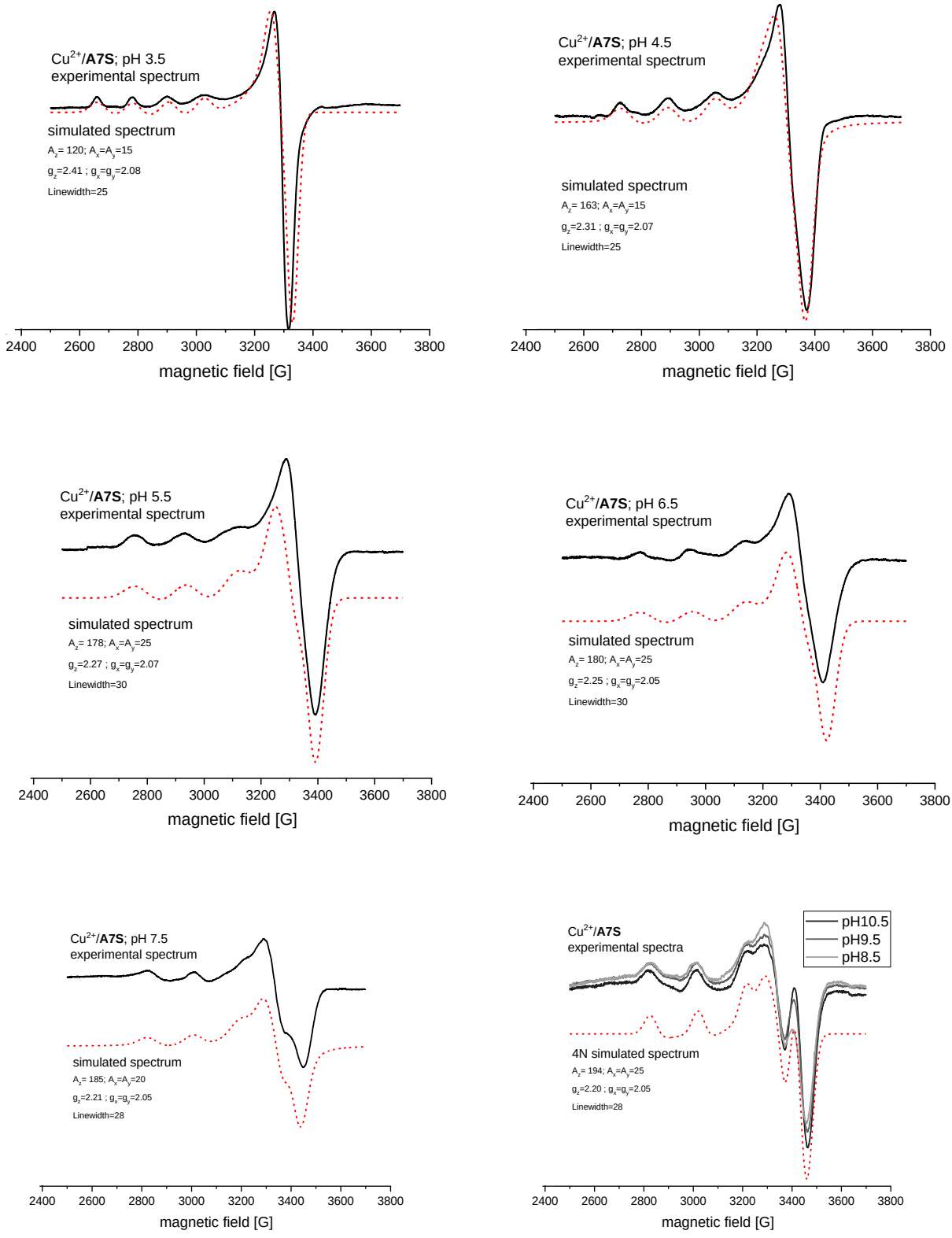

Figure S11. X-band EPR spectra of frozen solution (77K) of Cu^{2+} complexes with **A7S** at different pH values, *I*=0.1 M (KCl), M:L ratio 0.8:1, C_M = 1.00·10^{-3} M. Black solid line = experimental spectrum; red dashed line = simulated spectrum.

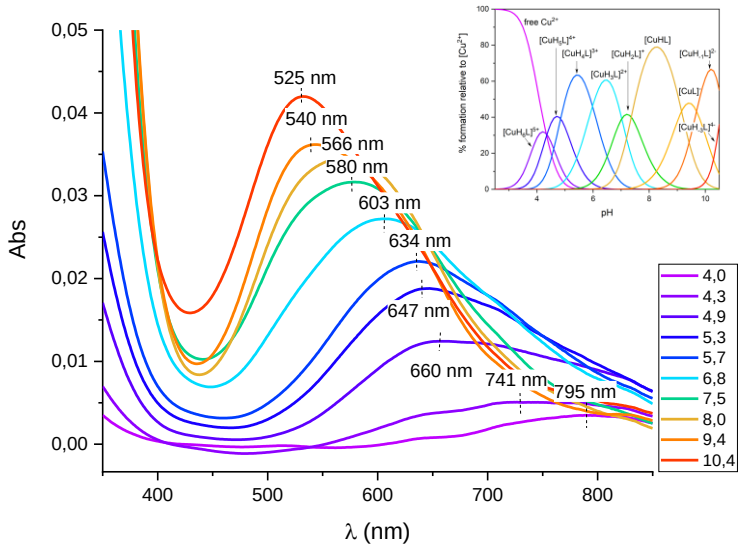

Figure S12. Vis absorption spectra of Cu^{2+} complexes with **A8S** at different pH values; M:L 0.8:1. C_M = 0.30·10^{-3} M, optical path 1 cm. The wavelength of maximum absorption is reported for each Vis absorption spectrum.

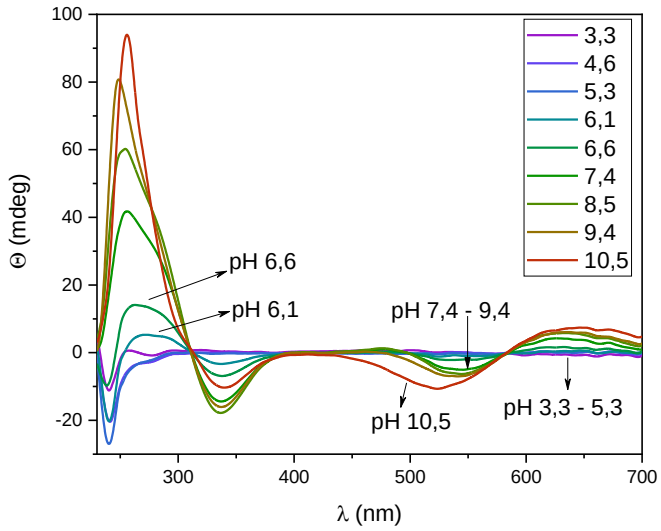

Figure S13. CD spectra of Cu^{2+} complexes with **A8S** at different pH values; M:L ratio 0.8:1, C_M=0.40·10^{-3} M, optical path 1cm.

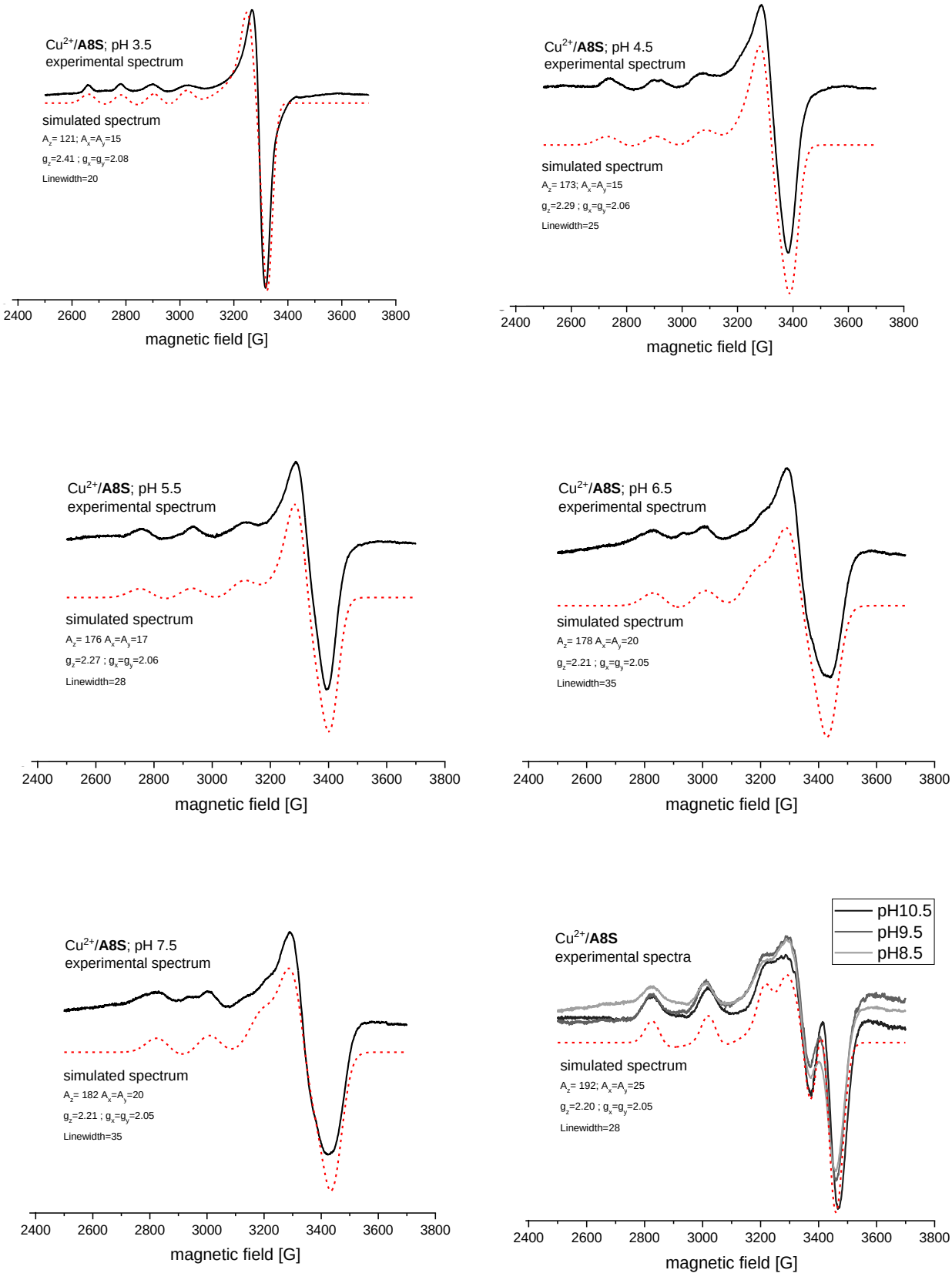

Figure S14. X-band EPR spectra of frozen solution (77K) of Cu^{2+} complexes with **A8S** at different pH values, *I*=0.1 M (KCl), M:L ratio 0.8:1, C_M = 1.00·10^{-3} M. Black solid line = experimental spectrum; red dashed line = simulated spectrum.

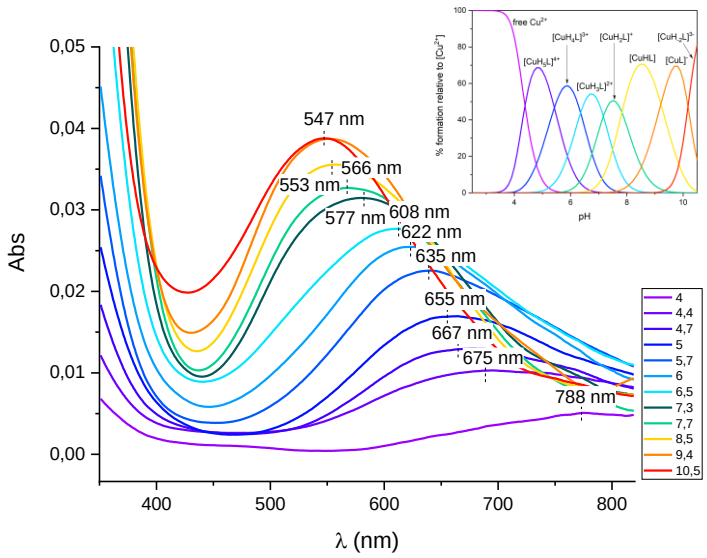

Figure S15. Vis absorption spectra of Cu^{2+} complexes with **A7S/A8S** at different pH values; M:L 0.8:1. $C_M = 0.30 \cdot 10^{-3}$ M, optical path 1 cm. The wavelength of maximum absorption is reported for each Vis absorption spectrum.

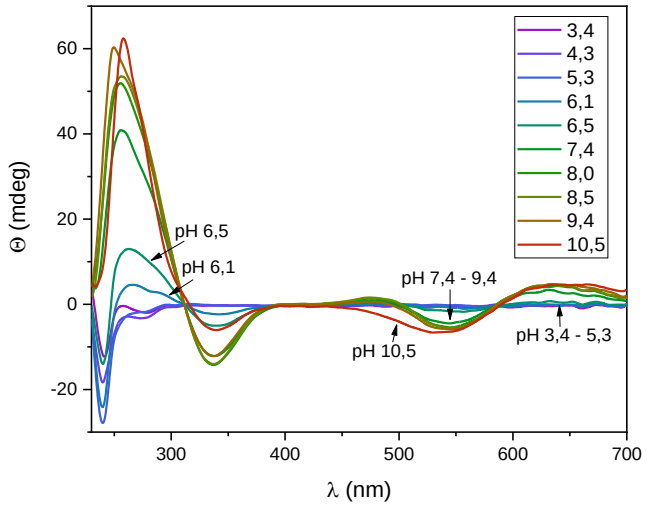

Figure S16. CD spectra of Cu^{2+} complexes with **A7S/A8S** at different pH values; M:L ratio 0.8:1, $C_M = 0.40 \cdot 10^{-3}$ M, optical path 1cm.

Figure S17. X-band EPR spectra of frozen solution (77K) of Cu^{2+} complexes with **A7S/A8S** at different pH values, *I*=0.1 M (KCl), M:L ratio 0.8:1, $C_M = 1.00 \cdot 10^{-3}$ M. Black solid line = experimental spectrum; red dashed line = simulated spectrum.

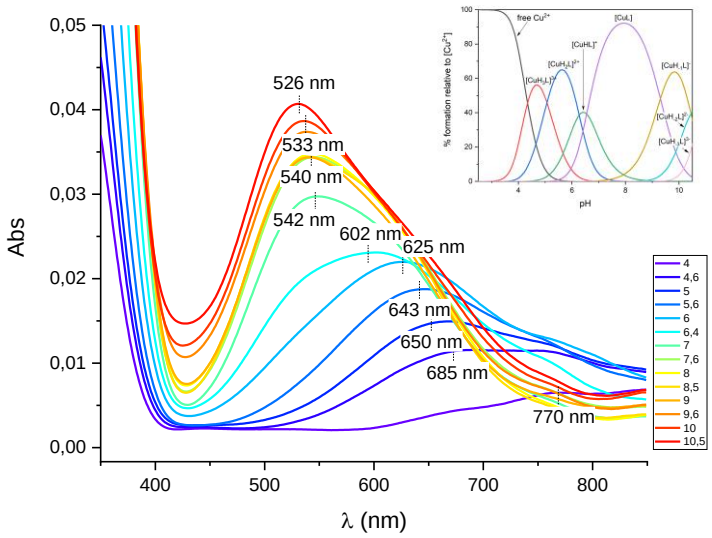

Figure S18. Vis absorption spectra of Cu^{2+} complexes with **WT(8-15)** at different pH values; M:L 0.8:1. $C_M = 0.30 \cdot 10^{-3}$ M, optical path 1 cm. The wavelength of maximum absorption is reported for each Vis absorption spectrum.

Table S3. EPR parameters for Cu^{2+} complexes with the studied peptides at I=0.1 M (KCl) and M:L molar ratio = 0.8:1. $C_L = 1.00 \cdot 10^{-3}$ M.

pH	A7S					A8S					A7/8S				
	$A_{//}$ [G] (A_z)	$g_{//}$ (g_z)	$g_{\perp}$ (g_x=g_y)	MW Frequency [GHz]	Coordinated N	$A_{//}$ [G] (A_z)	$g_{//}$ (g_z)	$g_{\perp}$ (g_x=g_y)	MW Frequency [GHz]	Coordinated N	$A_{//}$ [G] (A_z)	$g_{//}$ (g_z)	$g_{\perp}$ (g_x=g_y)	MW Frequency [GHz]	Coordinated N
3.5	120	2.41	2.08	9.60	-	121	2.41	2.08	9.60	-	118	2.41	2.08	9.60	-
4.5	163	2.31	2.07	9.60	2	173	2.29	2.06	9.60	2	160	2.31	2.07	9.60	2
5.5	178	2.27	2.07	9.60	3	176	2.27	2.06	9.60	3	170	2.28	2.06	9.60	2-3
6.5	180	2.25	2.05	9.60	3	178	2.21	2.05	9.60	3	176	2.26	2.06	9.60	3
7.5	181	2.21	2.05	9.60	3-4	182	2.21	2.05	9.60	3-4	184	2.21	2.05	9.60	3
8.5	189	2.20	2.05	9.60	4	190	2.20	2.05	9.60	4	194	2.20	2.05	9.60	4
9.5	190	2.20	2.05	9.60	4	190	2.20	2.05	9.60	4	194	2.20	2.05	9.60	4
10.5	194	2.20	2.05	9.60	4	192	2.20	2.05	9.60	4	194	2.20	2.05	9.60	4

4. Far UV circular dichroism

(A) (B) (C)

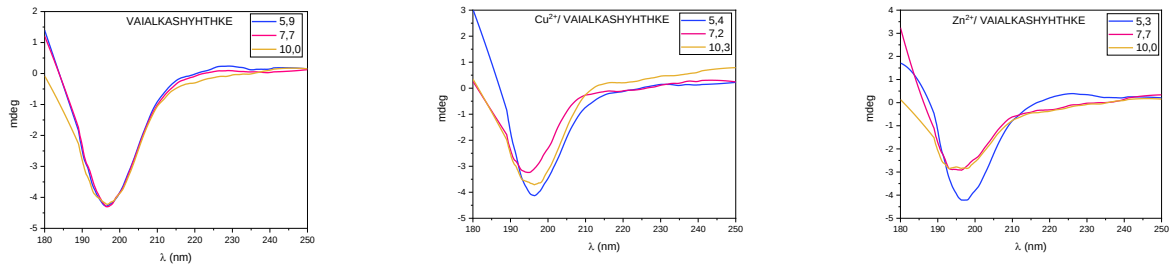

Figure S19. Comparison of CD spectra of (A) **A8S** and its (B) Cu^{2+} and (C) Zn^{2+} complexes at *T*=298 K, *I*= 0.1 M (KCl) in aqueous solution, M:L ratio 1:0.8, $C_M=0.08\cdot10^{-3}$ M, optical path 0.01 cm.

(A) (B) (C)

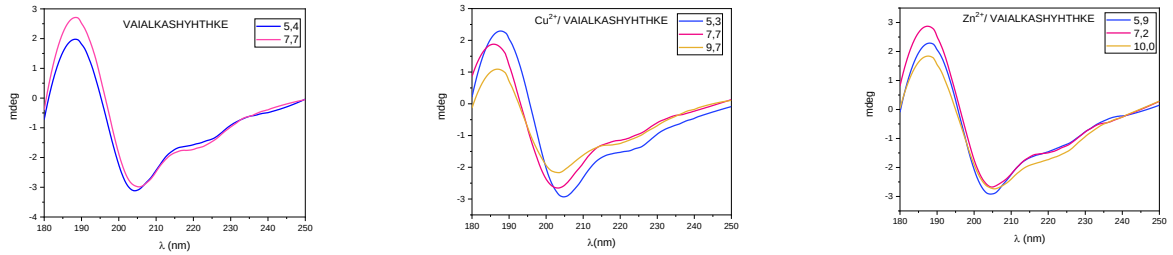

Figure S20. Comparison of CD spectra of (A) **A8S** and its (B) Cu^{2+} and (C) Zn^{2+} complexes at *T*=298 K, *I*= 0.1 M (KCl) in sodium dodecyl sulfate = $10\cdot10^{-3}$ M, M:L ratio 1:0.8, $C_M=0.08\cdot10^{-3}$ M, optical path 0.01 cm.

5. Mass spectrometry

Table S4. Stoichiometry, molecular formula and average *m/z* value for the species present in ESI-MS spectra of Cu^{2+} and Zn^{2+} complexes with the studied ligands; L:M molar ratio = 1:1 in MeOH:H_2O (1:1) mixture solution.

	Species	Formula	Average *m/z*
A7S	H_5L^{2+}	C77H123N23O21	853.0
Positive mode	$(H_4L \cdot K)^{2+}$	C77H122N23O21K	871.9
	$[CuH_3L]^{2+}$	C77H121N23O21Cu	883.4
	$([CuH_2L] \cdot K)^{2+}$	C77H120N23O21CuK	903.4
	$[ZnH_3L]^{2+}$	C77H121N23O21Zn	883.9
	$([ZnH_2L] \cdot K)^{2+}$	C77H120N23O21ZnK	902.9
A8S	H_5L^{2+}	C77H123N23O21	853.0
Positive mode	$(H_3L \cdot K_2)^{2+}$	C77H121N23O21K2	890.9
	$[CuH_3L]^{2+}$	C77H121N23O21Cu	883.4
	$([CuH_2L] \cdot K)^{2+}$	C77H120N23O21CuK	903.4
	$[ZnH_3L]^{2+}$	C77H121N23O21Zn	884.9
	$([ZnH_2L] \cdot K)^{2+}$	C77H120N23O21ZnK	903.9
A7S/A8S	H_5L^{2+}	C77H123N23O22	861.0
Positive mode	$(H_4L \cdot K)^{2+}$	C77H122N23O21K	879.9
	$[CuH_3L]^{2+}$	C77H121N23O21Cu	891.4
	$([CuH_2L] \cdot K)^{2+}$	C77H120N23O21CuK	911.4
	$[ZnH_3L]^{2+}$	C77H121N23O21Zn	891.9
	$([ZnH_2L] \cdot K)^{2+}$	C77H120N23O21ZnK	910.9

A)

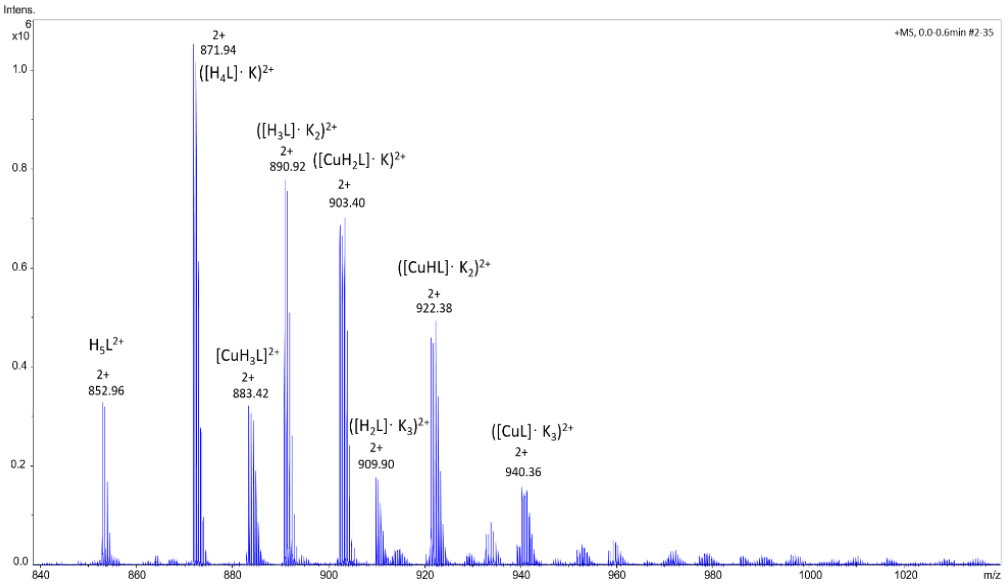

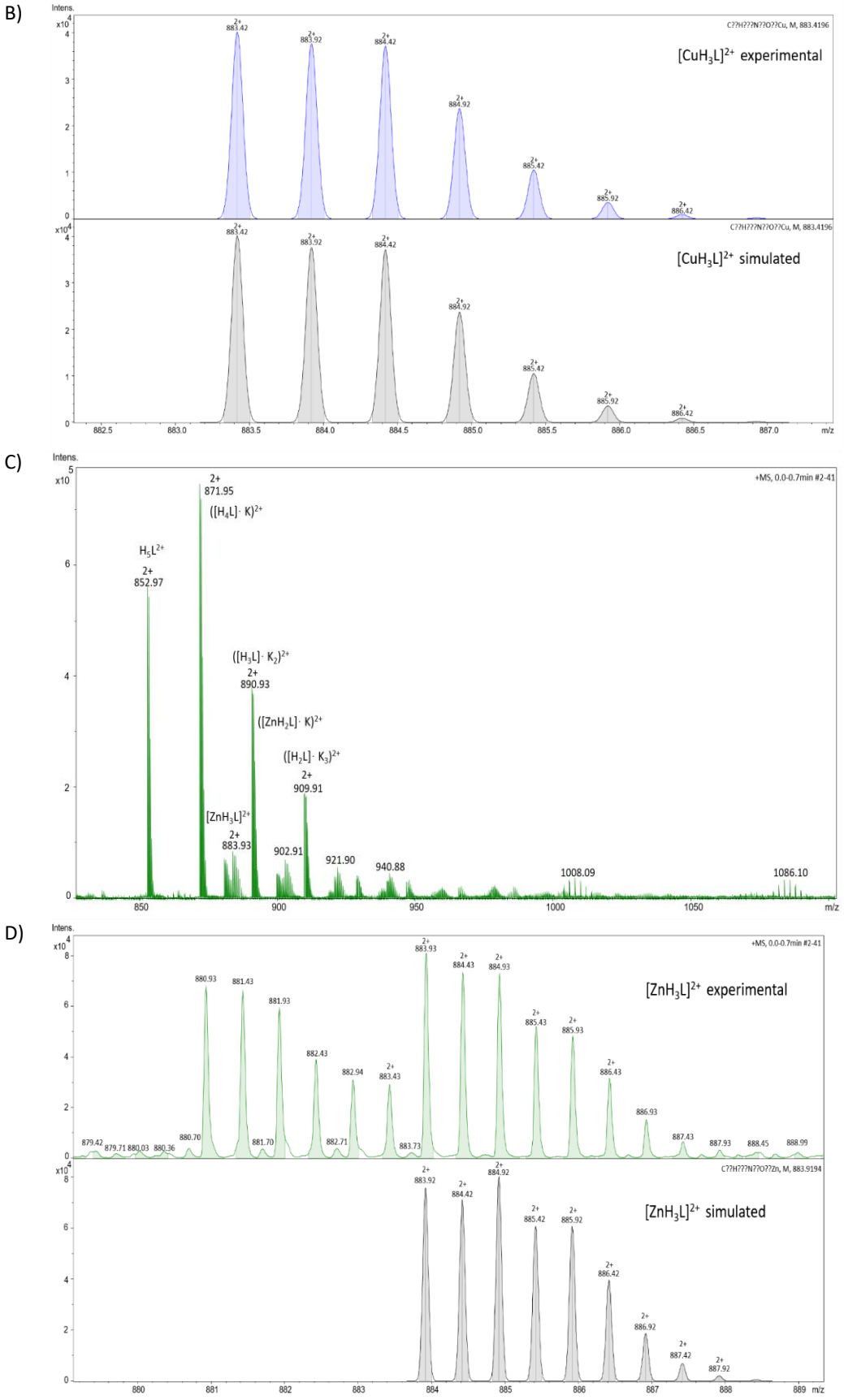

Figure S21. (A) ESI-MS spectrum for Cu^{2+}/ **A7S** system at L:M molar ratio=1:0.8 in MeOH:H_2O (1:1) mixture solution. (B) Comparison of experimental and simulated isotopic pattern of the chosen metal complex $[CuH_3L]^{2+}$. (C) ESI-MS spectrum for Zn^{2+}/ **A7S** system at L:M molar ratio=1:0.8 in MeOH:H_2O (1:1) mixture solution. (D) Comparison of experimental and simulated isotopic pattern of the chosen metal complex $[ZnH_3L]^{2+}$.

A)

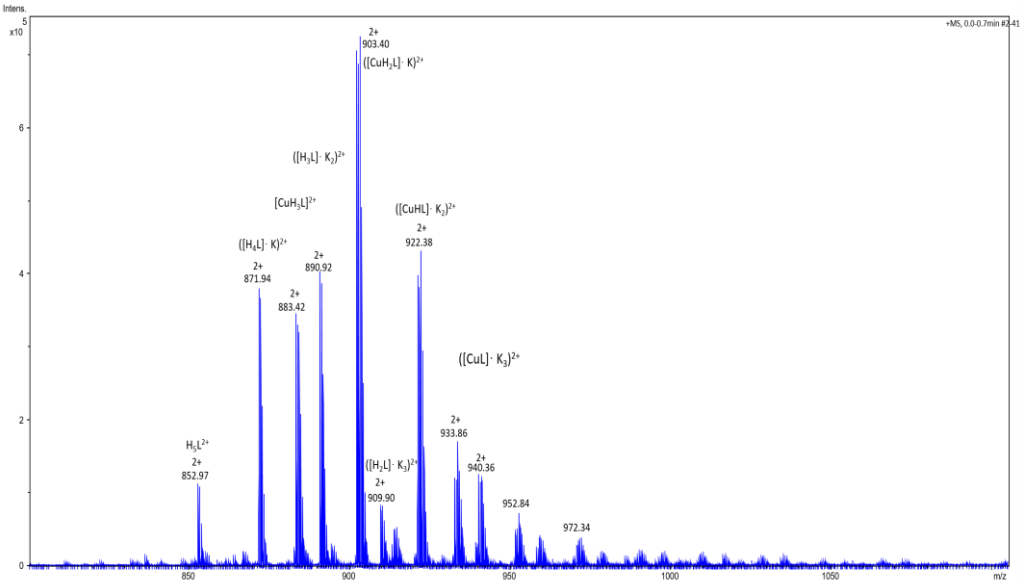
Intens.
x10
+MS, 0.0-0.7min #2-41
2+
903.40
([CuH3L]· K)2+
([H3L]· K2)2+
[CuH3L]2+
([CuHL]· K2)2+
([H4L]· K)2+
2+
922.38
2+
871.94
2+
890.92
2+
883.42
([CuL]· K3)2+
H5L2+
2+
852.97
2+
933.86
2+
940.36
([H2L]· K3)2+
2+
909.90
952.84
972.34
m/z

B)

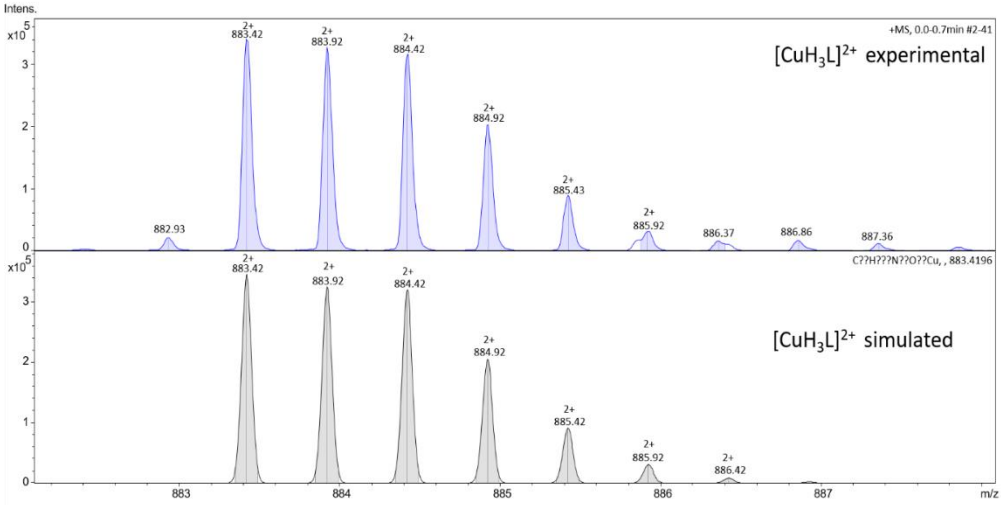
Intens.
x10
+MS, 0.0-0.7min #2-41
[CuH3L]2+ experimental
2+
883.42
2+
883.92
2+
884.42
2+
884.92
2+
885.43
2+
885.92
882.93
886.37
886.86
887.36
C??H???N??O??Cu, , 883.4196
[CuH3L]2+ simulated
2+
885.42
2+
886.42
m/z

C)

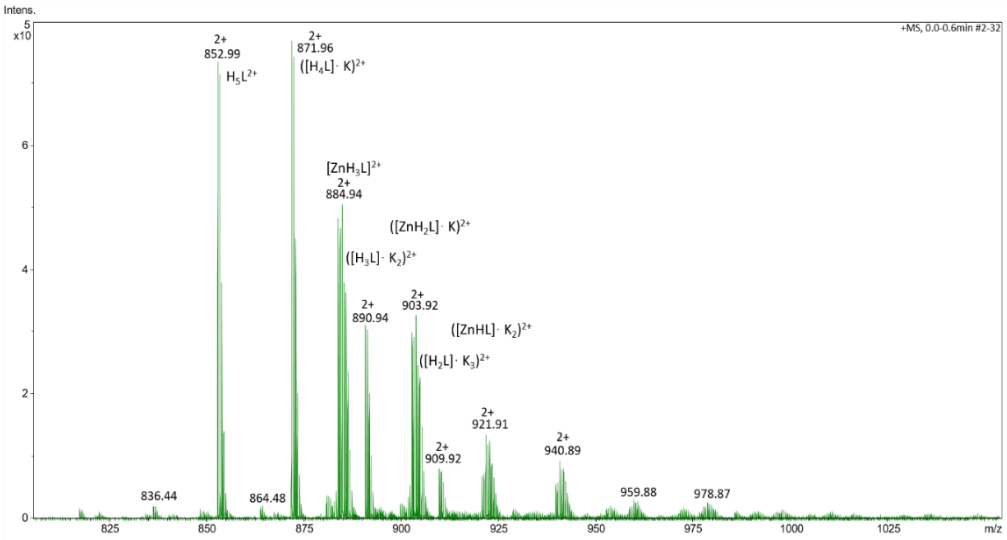
Intens.
x10
+MS, 0.0-0.6min #2-32
2+
852.99
H5L2+
2+
871.96
([H4L]· K)2+
[ZnH3L]2+
2+
884.94
([ZnH2L]· K)2+
([H3L]· K2)2+
2+
890.94
2+
903.92
([ZnHL]· K2)2+
([H2L]· K3)2+
2+
921.91
2+
909.92
2+
940.89
836.44
864.48
959.88
978.87
m/z

D)

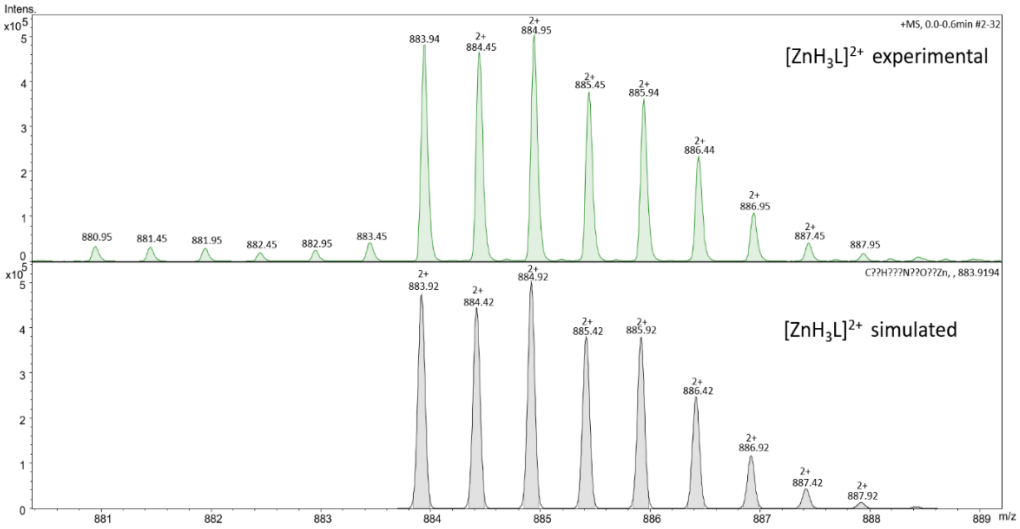

Figure S22. (A) ESI-MS spectrum for Cu^{2+}/ **A8S** system at L:M molar ratio=1:0.8 in MeOH:H_2O (1:1) mixture solution. (B) Comparison of experimental and simulated isotopic pattern of the chosen metal complex $[CuH_3L]^{2+}$. (C) ESI-MS spectrum for Zn^{2+}/ **A8S** system at L:M molar ratio=1:0.8 in MeOH:H_2O (1:1) mixture solution. (D) Comparison of experimental and simulated isotopic pattern of the chosen metal complex $[ZnH_3L]^{2+}$.

A)

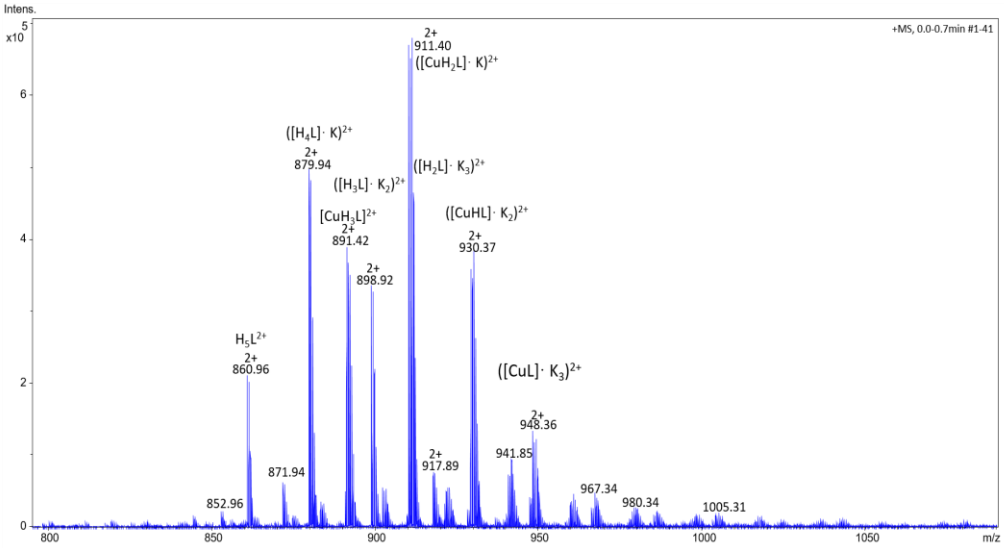

B)

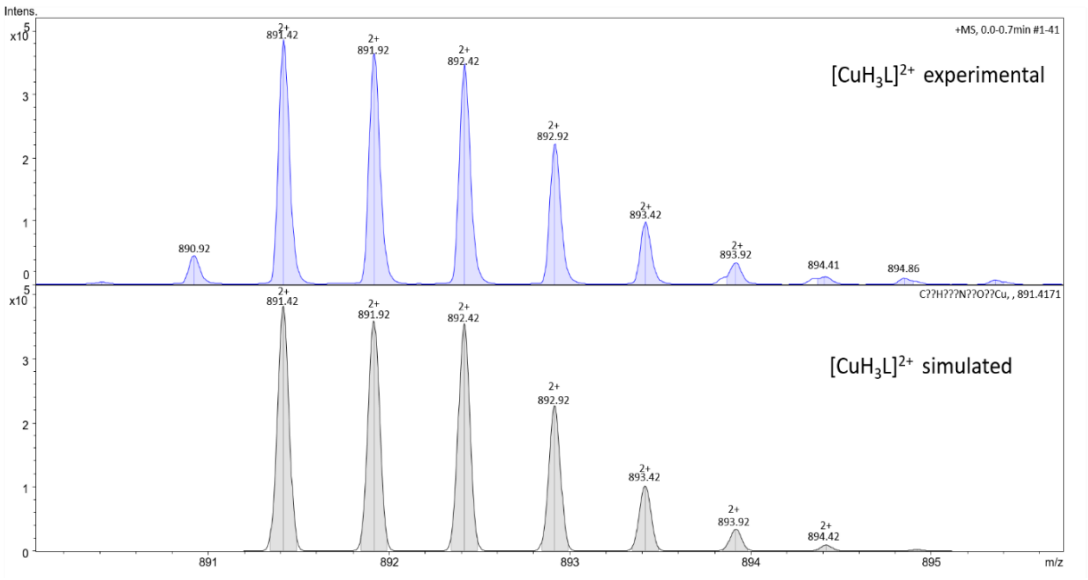

C)

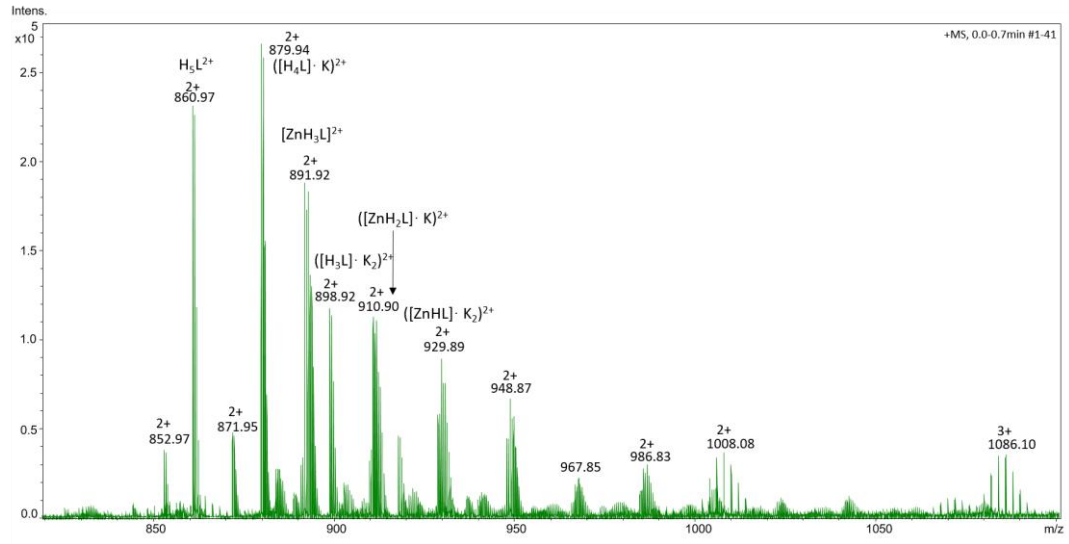

D)

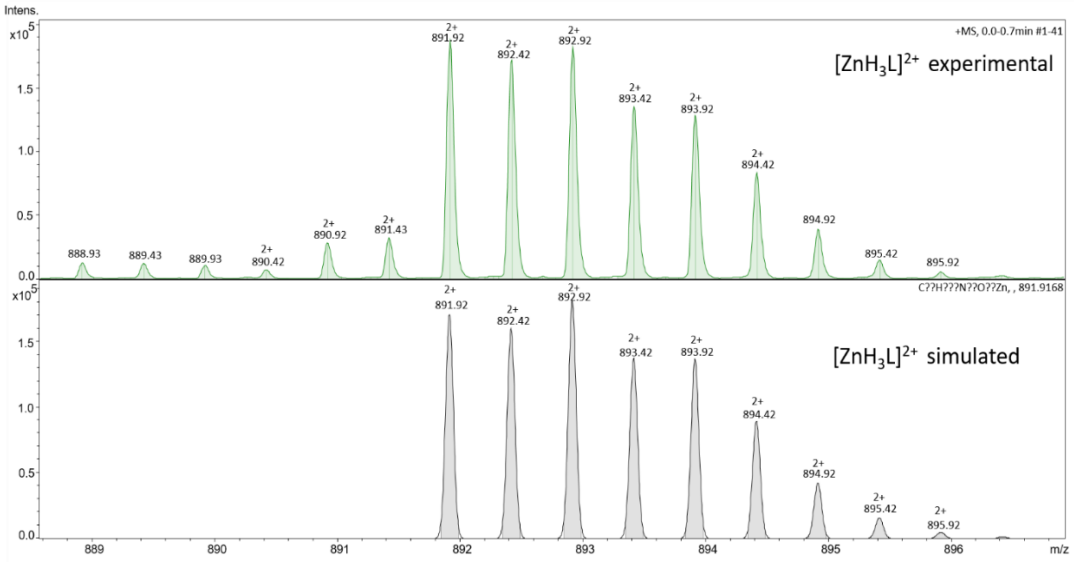

Figure S23. (A) ESI-MS spectrum for Cu^{2+}/ **A7S/A8S** system at L:M molar ratio=1:0.8 in MeOH:H_2O (1:1) mixture solution. (B) Comparison of experimental and simulated isotopic pattern of the chosen metal complex $[CuH_3L]^{2+}$. (C) ESI-MS spectrum for Zn^{2+}/ **A7S/A8S** system at L:M molar ratio=1:0.8 in MeOH:H_2O (1:1) mixture solution. (D) Comparison of experimental and simulated isotopic pattern of the chosen metal complex $[ZnH_3L]^{2+}$.

6. Stability of peptide-metal complexes

The competition diagrams in Figure S22 allow us to compare the metal binding ability of the fragment **WT(8-15)** with wild-type calcitermin **WT**[1] and its terminal protected analogue, Ac-VAIALKAAHYHTHKE-NH_2;[1] these competition plots give information on the possible contribution of residues 1–7 in the stabilization of metal complexes, even if they are not directly involved in coordination. Furthermore, the comparison allows us to evaluate the impact of the amino- and carboxyl-terminal groups in the complexation of the metal ion. In the whole pH range, in the case of copper, wild-type calcitermin presents the best metal binding affinity. This behavior can be explained by the presence of the free terminal groups, in particular the terminal amino group, which are available as donor groups able to coordinate the metal ion. The competition diagram shows that the short fragment **WT(8-15)** coordinates copper ion with less efficacy even compared to the protected calcitermin (Ac-VAIALKAAHYHTHKE-NH_2), although the proposed coordination modes are the same for both the systems. This behavior opens the way to the hypothesis (which would require support from quantum mechanical calculations and molecular dynamics studies) that the N-terminal hydrophobic domain of calcitermin contributes to the stability of the complexes, protecting the metal from solvent interference, for example through long-range non-bonding interactions or forming a sort of "hydrophobic cage" around copper ion. In the case of zinc, wild-type calcitermin is again the best ligand, most likely due to the presence of the free carboxyl and amino terminal groups, which also confer a different net charge to the peptide. This may have an effect on the stability of the formed complexes, and therefore justify the higher metal-binding affinity. The lipophilic N-terminal fragment, however, does not exert a stabilization effect as in the case of copper, since **WT(8-15)** is able to chelate zinc ion better than Ac-VAIALKAAHYHTHKE-NH_2. This is not surprising, considering that zinc is able to bind up to two solvent molecules and form stable complexes at pH higher than 7.

(A) **(B)**

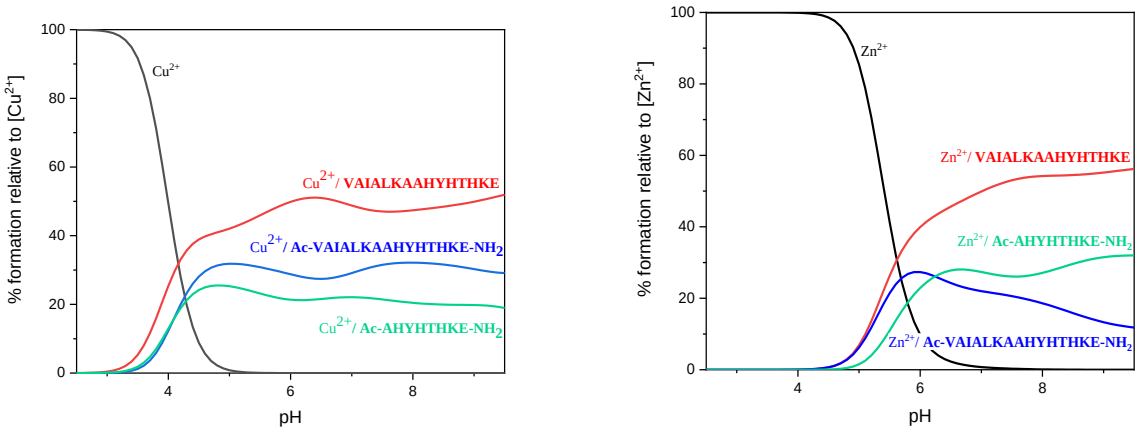

Figure S24. Competition plots for a simulated solution containing equimolar concentrations of (A) Cu^{2+}, (B) Zn^{2+}, and **WT,**[1] Ac-VAIALKAAHYHTHKE-NH_2,[1] and Ac-AHYHTHKE-NH_2 (**WT(8-15)**).

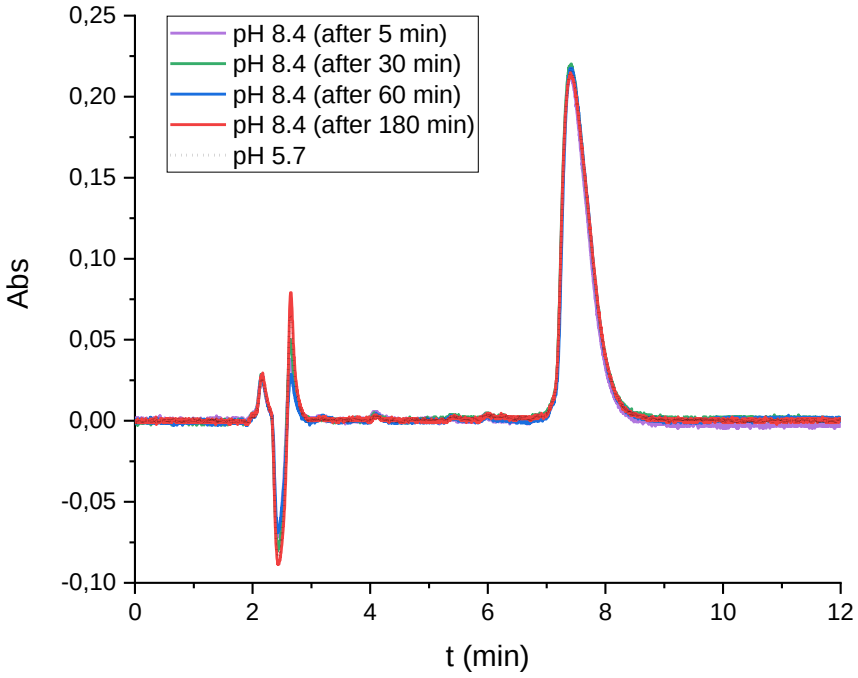

Figure S25. Chromatograms of a solution containing Cu^{2+}/VAIALKSSHYHTHKE (M:L ratio = 1:1; C_L=0.5 mM) at pH 5.7 (dotted line) and 8.4 (solid lines) registered after different times, T = 25 °C. The analytical column was an Agilent Poroshell 120 SB-C18 (4.6 x 100 mm, 2.7 µm, pore size 120 Å). Flow rate = 0.5 ml/min, mobile phase H_2O: acetonitrile = 83:17 + 0.1% v/v TFA, isocratic elution, T=25 °C, detection wavelength 214 nm.

7. References

1. M. D'Accolti, D. Bellotti, E. Dzień, C. Leonetti, S. Leveraro, V. Albanese, E. Marzola, R. Guerrini, E. Caselli, M. Rowińska-Żyrek and M. Remelli, *Sci. Rep.*, 2023, **13**, 18228.
2. H. Sigel and R. B. Martin, *Chem. Rev.*, 1982, **82**, 385-426.
3. E. Prenesti, P. G. Daniele, M. Prencipe and G. Ostacoli, *Polyhedron*, 1999, **18**, 3233-3241.